The July 2019 Ridgecrest, California, Earthquake Sequence Recorded by Creepmeters: Negligible Epicentral Afterslip and Prolonged Triggered Slip at Teleseismic Distances

Roger Bilham*1 and Bryan Castillo2

Abstract

We report sequential triggered slip at 271–384 km distances on the San Andreas, Superstition Hills, and Imperial faults with an apparent travel-time speed of 2.2 \pm 0.1 km/s, following the passage of surface waves from the 4 July 2019 (17:33:49 UTC) $M_{\rm w}$ 6.4 and 6 July 2019 (03:19:53 UTC) $M_{\rm w}$ 7.1 Ridgecrest earthquakes. Slip on remote faults was not triggered instantaneously but developed over several minutes, increasing in duration with distance. Maximum slip amplitudes varied from 10 μ m to 5 mm within minutes of slip nucleation, but on the southernmost San Andreas fault slip continued for two months and was followed on 16 September 2019 by a swarm of microearthquakes ($M_{\rm w} \leq$ 3.8) near Bombay Beach. These observations add to a growing body of evidence that fault creep may result in delayed triggered seismicity. Displacements across surface faults in the southern epicentral region and on the Garlock fault in the months following the Ridgecrest earthquakes were negligible (<1.1 mm), and they are interpreted to characterize surface strain adjustments in the epicentral region, rather than to result from discrete slip on surface faults.

Cite this article as Bilham, R., and B. Castillo (2020). The July 2019 Ridgecrest, California, Earthquake Sequence Recorded by Creepmeters: Negligible Epicentral Afterslip and Prolonged Triggered Slip at Teleseismic Distances, Seismol. Res. Lett. 91, 707–720, doi: 10.1785/0220190293.

Introduction

Eleven extensometers at nine locations were operating in southern California during the Ridgecrest earthquakes of 4 and 6 July 2019, and seven new instruments were installed on the Ridgecrest ruptures and on the nearby Garlock fault after the earthquake (Fig. 1). Each of these extensometers, in addition to one near Hollister, was of similar design (described subsequently) with a resolution of 2 μ m and a recording rate of 1 sample per minute. The U.S. Geological Survey (USGS) creepmeters operating in central California and the Bay Area at distances beyond 290 km from the Ridgecrest earthquakes have lower resolution and a 10 min recording rate and did not record significant offsets during the earthquakes.

The article first describes the instruments used and then proceeds to quantify triggered slip on the San Andreas, Superstition Hills, and Imperial faults. A succeeding section discusses results from the rapid deployment of extensometers across the southern (publicly accessible) ends of the Ridgecrest ruptures and surface fissures along the Garlock fault, where displacements were unexpectedly modest (<0.5 mm in the two months after the earthquakes). A final section discusses aspects of triggered slip and unexpected changes in creep rate

induced by the earthquakes following triggered slip in the Mecca Hills and Durmid Hill in the Coachella Valley.

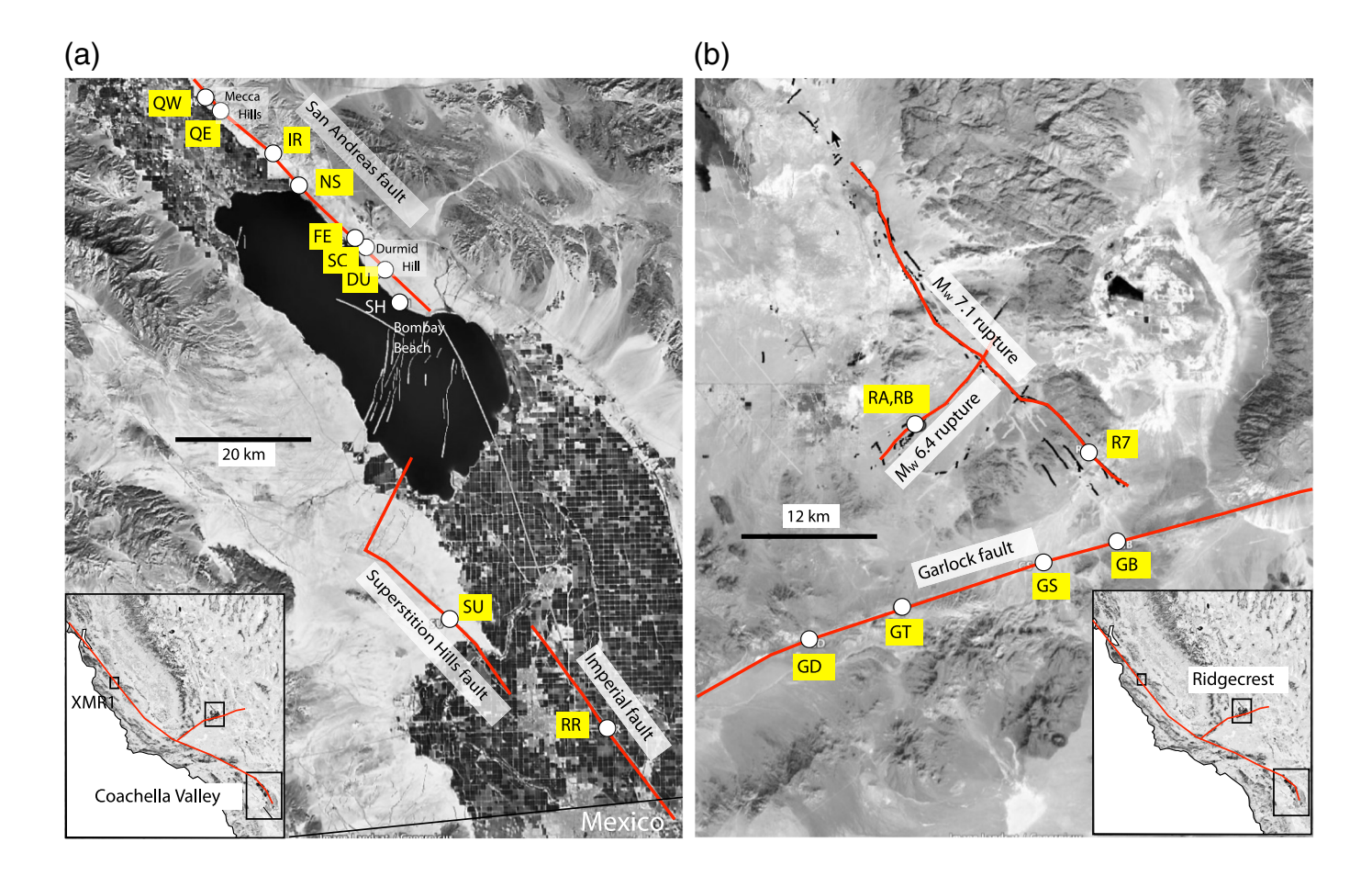
Creepmeter Instrumentation

With a few exceptions, each creepmeter discussed here is an extensometer that uses a 6 mm diameter carbon-fiber rod as a length standard, buried obliquely across the surface trace of an active fault (Fig. 2). The 3–20 m long rod slides within a 1.2 cm diameter telescopic conduit buried 30–50 cm deep across the fault, and one end is fastened rigidly to a buried steel tripod. The free end of the rod is held in 1 N tension by a 0.1 mm diameter, multistrand, stainless-steel wire wrapped once around the 3.175 mm diameter shaft of a 360° continuous rotation, Hall effect sensor with a linearity of <0.3%. The effective circumference of the shaft including a correction for the thickness of the 19 strand, nylon coated, stainless-steel wire is

Geological Sciences and CIRES, University of Colorado, Boulder, Colorado, U.S.A.;
 Department of Geological Sciences, California State University, San Bernardino,

^{*}Corresponding author: bilham@colorado.edu

[©] Seismological Society of America



approximately 10 mm. The free end of the wire is fed by a constant tension spring motor with 1-3 m of range. Slip on the fault pulls the rod through the conduit, which results in rotation of the shaft of the sensor. The resulting 0-5 volt 12 bit output is recorded by a 16 bit data logger yielding a fault-slip resolution of 2 μ m. Monotonic slip exceeding 10 mm resets the 0-5 V signal to zero, and hence the creepmeter has a wide cumulative measurement range, and, unless an earthquake with >1 m slip occurs, no adjustments are needed during its lifetime. Typically an extensometer can be installed by two people in 3 hr using just a shovel and a pick. Initial settlement is rapid, and stable readings are usually available within a day of installation. Despite their shallow burial (20-30 cm), temperature effects are small ($<2 \mu m/^{\circ}C/m$) due to the similar expansion coefficients of carbon-fiber composites and surface soils. Where telemetry is inadvisable due to potential vandalism, the creepmeter can be totally buried and will operate for a year from disposable alkaline batteries. To conserve power, the autonomous data logger switches the power to the sensor for 0.1 s once per minute, using a clock with a nominal accuracy of 1 min per month. Clock corrections accurate to a few seconds are obtained from the difference in the time stamp at the end of the recorded file and the creation time of the saved data, adjusted by an empirically determined file transfer delay. The timing of triggered slip data to a timing accuracy of 5 s in this article is based on clock drift incurred from ≈100 days

Figure 1. Locations of creepmeters in the Coachella Valley and Ridgecrest regions (Insets show Southern California). Coordinates are listed in Tables 1 and 3. Significant faults are named: white lines in are (a) faults from U.S. Geological Survey and California Geological Survey (2006). Black lines in are (b) faults mapped by Kendrick et al. (2019). The color version of this figure is available only in the electronic edition.

before, to 2 days after, the $M_{\rm w}$ 7.1 earthquake and assumes linear clock drift.

An obliquely installed extensometer is an imperfect measure of fault creep because it assumes that the two sides of the fault act as rigid blocks separated by an infinitely thin fault plane. If the length standard remains straight, fault creep = extension/cos(obliquity). In the extensometers described here, this geometry is approximated by a fault shear zone that after sufficient fault slip has occurred will impose an arctan curve on the initially straight rod. In practice, although the assumption of block-like motion is violated, ≈1% measurement accuracy can be obtained, because fault slip (5 mm) is typically much smaller than the width of the fault zone (e.g., 5 m). Creepmeters often underestimate fault-zone slip because the fault is frequently associated with a shear zone that extends beyond the aperture sensed by the instrument. In Tables 1–3 and accompanying figures we tabulate only the observed

extension and not the implied dextral slip, which is obtained by dividing by the cosine of the stated obliquity.

Although the mechanical arrangement described earlier results in a large dynamic range, it comes with a measurement penalty because of frictional components in the sensor that result in stiction. Stiction is a stick-slip instrumental artifact caused by friction between the rod and its conduit, and from the bearings in the Hall sensor and tensioning pulleys. In a newly installed instrument, these effects are observed to be less than 10 μ m, and when present occur with time durations of

Figure 2. Schematic view of the extensometers deployed to measure aseismic surface fault creep in this study. Arrows show sense of motion for fault-zone extension. The system is anchored at each end with three \approx 2 cm diameter rods driven to refusal at 1–2 m depth, clamped at their upper ends to a welded platform. The extensometer typically crosses the fault zone obliquely at a depth of 30–50 cm and at an angle of 30° (in an extensional sense) to the strike of the fault. The color version of this figure is available only in the electronic edition.

TABLE 1
Locations of Creepmeters and Amplitudes of Triggered Displacements (mm)

Site	North Latitude	West Longitude	М _w 6.4	М _w 7.1	Sum	Fault Segment
QW30	33.6526	116.0846	-0.002	4.323	4.321	West Quarry SSA Mecca Hills
QE30	33.6473	116.0780	0.294	3.682	3.976	East Quarry SSA Mecca Hills
IR30	33.5700	115.9785	0.001	-0.009	-0.009	Indian Ring SSA North Shore*
NS45	33.5307	115.9388	-0.101	-0.019	-0.120	North Shore SSA North Shore
FE30	33.4572	115.8539	0.054	0.394	0.448	Ferrum SSA Durmid Hill
SC30	33.4485	115.8437	0.294	0.654	0.949	Salt Creek SSA Durmid Hill
SC72	33.4485	115.8437	0.001	0.111	0.113	Salt Creek SSA Durmid Hill
DU30	33.4120	115.7950			<0.45	Pipeline SSA Durmid Hill
SH30	33.3713	115.7808			<0.3	North Shoreline Fault
SU30C	32.9303	115.7009	0	0.014	0.014	Superstition Hills
SU30I	32.9303	115.7009	0	0.029	0.029	Superstition Hills
RR45	32.7812	115.4485	-0.031	-0.078	-0.109	Ross Road, Imperial
XMR30	36.5920	121.1867	0.015	0.037	0.052	SA Melendy Ranch

The numbers following the two-letter site name in the first column indicate the obliquity of the creepmeter relative to the strike of the fault in degrees. NS45, SC72, and RR45 are creepmeters described in Louie et al. (1985) and McGill et al. (1989) refurbished with carbon rods and Hall sensors. The Superstition Hills creepmeters at Imler road are designated SU30I, an invar rod instrument installed in 1987 (Bilham, 1989), and SU30C a carbon rod instrument installed 2 m to its north in 2018. Southern San Andreas (SSA) fault segments are named as in Bilham and Williams (1985). XMR30 is a refurbished U.S. Geological Survey (USGS) instrument XMR1 south of Hollister described in Schulz (1989). Negative numbers in italics signify sinistral slip. DU30 and SH30 were inoperative for the earthquakes but maximum amplitude for triggered slip has been estimated from observations from before and after their missing data. SA, San Andreas fault.

^{*}Close to a point described by Shifflett et al. (2002).

less than 1 s. Offsets occur in the data at the time of downloading due to manual disturbances to the instrument; however, a truck may be driven over the buried instrument without inducing stiction jumps. Triggered fault slip, with amplitudes less than 60 μ m described in this article, can usually be distinguished from abrupt instrumental stiction, because fault slip is typically associated with durations of several minutes.

Data

Two days after the $M_{\rm w}$ 7.1 Ridgecrest earthquake, creep data were downloaded manually from nine locations in southern California (Fig. 1a and Table 1). On the third day, a creepmeter was installed on the western branch of the $M_{\rm w}$ 6.4 Ridgecrest rupture, and, in the subsequent two weeks, six additional creepmeters were assembled and installed across the southern end of the $M_{\rm w}$ 7.1 rupture and on the Garlock fault (Fig. 1). Data from these sensors, and from XMR1 near Hollister, are illustrated in Figures 3 and 4, and their time series may be accessed from the UNAVCO data archive. As previously mentioned, strike-slip offsets are obtained by dividing listed values for extension indicated in Tables 1 and 3 by the cosine of the instrument obliquity.

Maximum slip of 0.45 mm has been inferred at DU30 from secular trends before and after a data gap from 12 June to 9 July caused by a power supply failure (Fig. 3h). Four other creepmeters on faults near Yuha (Rymer et al., 2011), on the San Jacinto, and the Shoreline fault (SH in Fig. 1) (Jänecke et al., 2018) had been mothballed prior to the earthquakes due to an absence of operational funds; however, March-September static values at SH provided a weakly constrained maximum amplitude for slip triggered in the Ridgecrest earthquakes (0.3 mm), and the site was reactivated following a microearthquake swarm near Bombay Beach in late September 2019.

During data collection in the Mecca Hills, we observed a suite of en echelon fissures that had developed along the 870 m long surface trace of the San Andreas fault between the two creepmeters QW and QE and extending an unknown distance beyond them. No surface cracking was observed near creepmeters elsewhere, consistent with previous observations that fault-zone cracks are manifest only where creep exceeds 3 mm (Bilham, 2005). Surface cracks, however, were reported near a paleoseismic trench (33.446° N, 115.840° W, G. Seitz, written comm., 2019) south of Salt Creek. The style and physical appearance of these en echelon cracks is identical to those found in the Ridgecrest meizoseismal region.

Amplitudes of Triggered Slip

In general, the maximum amplitude of triggered slip decays with distance from the Ridgecrest earthquakes, but the amount of slip depends also on the structural setting of each segment of the fault and the recent history of local aseismic slip (Fig. 3). The largest observed slip was in the northwest Mecca Hills (4.3 mm extension, 5 mm dextral slip, Fig. 3b), with an order of magnitude less slip on Durmid Hill. Negligible slip occurred on the intervening North Shore segment, consistent with its historical behavior (Bilham and Williams, 1985). In 2017, significant aseismic slip was observed in the southeast Mecca Hills (Tymofyeyeva et al., 2019), but not in the northwest Mecca Hills at the location where maximum slip was triggered in 2019.

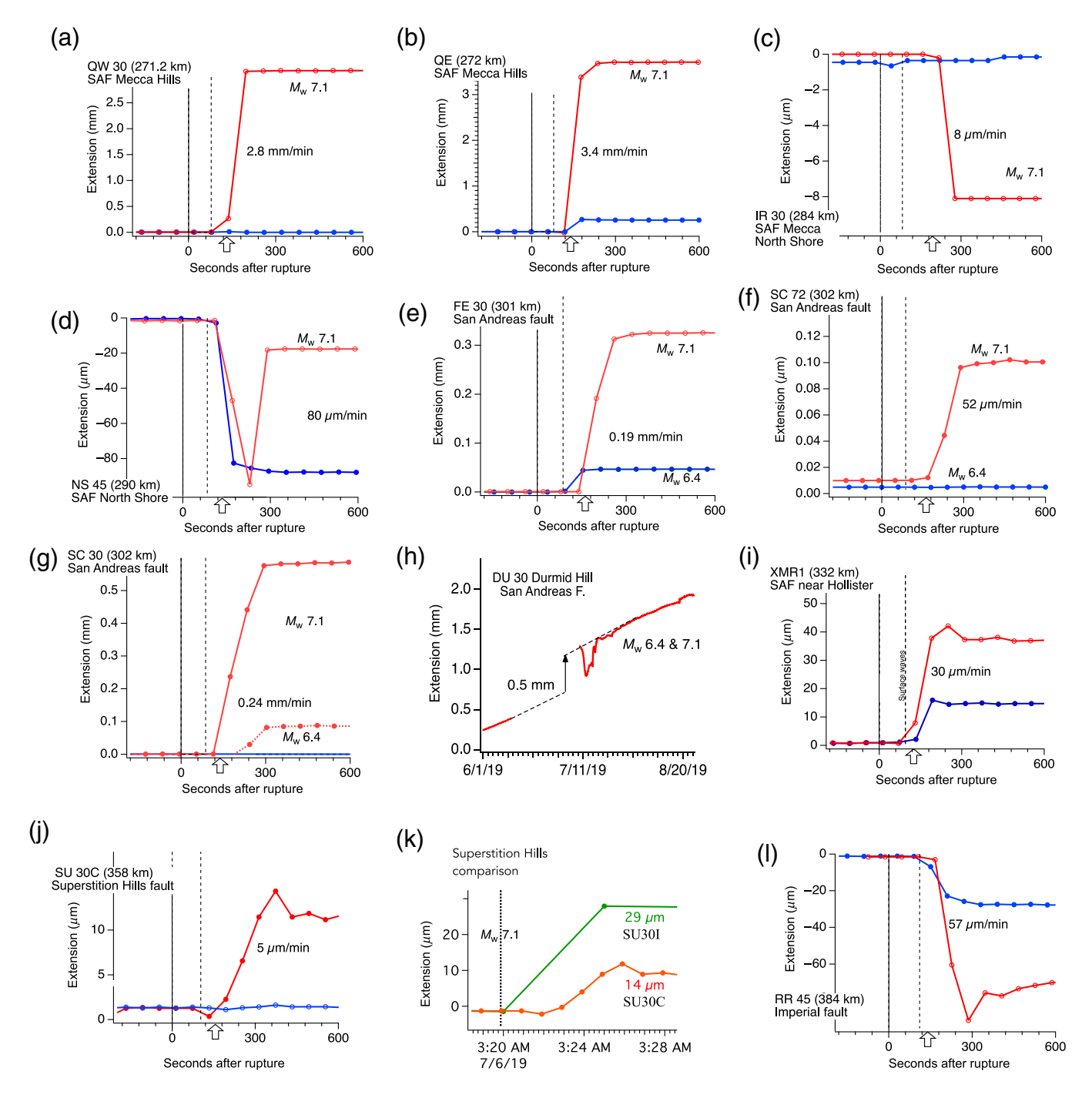
The amplitudes of slip recorded elsewhere were small compared to previous reports of triggered slip (e.g., Cohn et al., 1982; Louie et al., 1985; Bodin et al., 1994; Rymer et al., 2011; Wei et al., 2011, 2015), but despite their small amplitude appear to be meaningful at the $\pm 10~\mu m$ level. For example, two independent creepmeters on the Superstition Hills fault, 2 m apart and with different length standards, sensors, and recording systems recorded synchronous 14 and 29 µm dextral offsets following the $M_{\rm w}$ 7.1 earthquake (Fig. 3k). The mean slip velocity recorded by the Invar-linear variable differential transformer system (5 min sample rate) was 6 μ m/ min compared to the maximum velocity on the carbon system of 5 μ m/ min, 3-4 min after the onset of triggered slip.

Net sinistral slip (<0.1 mm, Fig. 3c,d) was recorded by creepmeters at the northwest and southeast ends of the San Andreas North Shore segment (IR and NS). This sense of motion was unexpected, and their polarities were subsequently checked and confirmed. The creepmeter at Ross Road on the Imperial fault also recorded sinistral slip following both the $M_{\rm w}$ 6.4 and 7.1 earthquakes (Fig. 31), and in this case the reason is attributable to the sense of slip recorded prior to the earthquakes. Between early June and mid-July, an almost linear sinistral signal (7 μ m/day) was recorded on the Imperial fault at Ross Road, apparently the result of desiccation following local changes in irrigation. Sinistral slip triggered by the Ridgecrest earthquakes here was equivalent in amplitude to 15 days of slow sinistral slip prior to and following the earthquakes.

The two Ridgecrest earthquakes occurred 33.8 hr apart, and at each extensometer triggered slip was larger for the second event. Assuming that dynamic triggering occurs during transient Coulomb failure conditions suited to partially releasing shear strain near a fault as envisaged by Wei et al. (2015) and Tymofyeyeva et al. (2019), the surface waves from the $M_{\rm w}$ 6.4 event incompletely released this strain, and the larger amplitude surface waves from the $M_{\rm w}$ 7.1 released additional shear strain. We discuss the implications of this later.

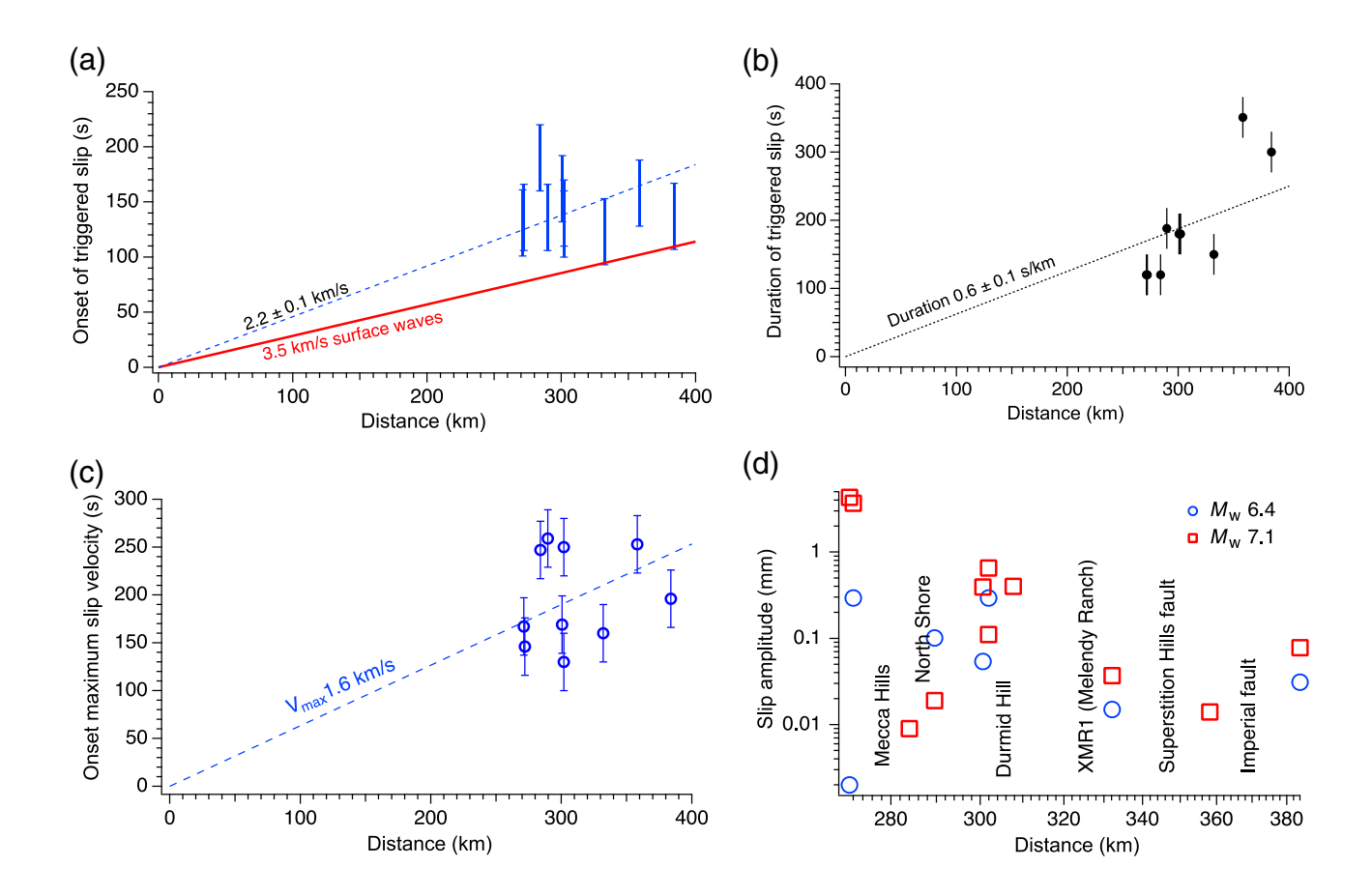
Triggered Slip Onset and Duration in the Coachella and Imperial Valleys

Surface waves swept past the creepmeters 270-380 km from the Ridgecrest epicenters starting between 1.3 and 1.8 min after the origin time. Although sampling time is estimated accurate to 5 s, the data loggers sample slip at one-minute intervals, which limits the accuracy of time picks. A travel-time graph shows that fault slip develops after the arrival of surface waves propagating at 3.5 km/s (a least-squares fit travel-time velocity



of 2.2 ± 0.1 km/s) (Fig. 4a). The time of maximum dextral slip velocity on the fault is also delayed and increases with distance with an effective propagation velocity of 1.6 km/s. At none of the sites was slip complete in less than one minute, with a maximum duration of 6 min on the Imperial fault close to the Mexican border (Table 2). A graph of this increasing duration shows it to increase with teleseismic distance at a rate of 0.6 ± 0.1 s/km (Fig. 4b,c). This is broadly consistent with the findings of Wei *et al.* (2015) and Tymofyeyeva *et al.* (2019) who show that failure criteria during dynamic triggering are responsive to peaks in the maximum amplitudes of surface waves, which may exceed threshold triggering values several cycles after the first arrival of surface waves.

Figure 3. Data from three minutes before, to 10 min after the origin time of the $M_{\rm w}$ 6.4 (blue) and $M_{\rm w}$ 7.1 (red) earthquakes with maximum observed fault-slip velocities indicated. (a–l) Creepmeter data are plotted sequentially with increasing epicentral distance and named as in Figure 1 and Table 1. At each location, the $M_{\rm w}$ 7.1 earthquake triggered larger offsets. The line at zero is the origin time, the dashed line is the synthetic arrival time of surface waves (Table 2), and arrows indicate subjective picks of the onset time of triggered slip following the $M_{\rm w}$ 7.1 earthquake. (h) DU(30) was inoperative at the time of the earthquake, and its offset is interpolated. (k) Two independent extensometers on the Superstition Hills fault yield small but similar offsets following the $M_{\rm w}$ 7.1 earthquake. (d,i,j) Overshoot is recorded at three locations. The duration of triggered slip, in general, increases with epicentral distance. SAF, San Andreas fault. The color version of this figure is available only in the electronic edition.



Negligible Epicentral Afterslip

The first of seven extensometers was installed across surface ruptures in the epicentral region 5 days after the $M_{\rm w}$ 6.4 earthquake and three days after the $M_{\rm w}$ 7.1 earthquake. Ultimately two extensometers were located on the western end of the $M_{\rm w}$ 6.4 rupture and one on the southern end of the $M_{\rm w}$ 7.1 rupture. Naval facility restrictions prevented access to locations further north. Four extensometers were placed across the Garlock fault. The locations of these extensometers are listed in Table 3 and shown graphically in Figure 1b.

The siting of extensometers across the Ridgecrest ruptures with ≥ 1 m of slip was determined by avoiding major push-ups or pull-aparts, favoring instead locations where the fault zone was relatively narrow. A $\approx 30^{\circ}$ oblique path across the fault was then selected such that the instrument would undergo extension during strike-slip motion. The anchors for the extensometers were placed no closer than 1 m to the edge of the nearest fissure, and the length of the extensometer was determined by the width needed to embrace the furthest hairline cracks (Table 3).

In the case of the Garlock fault, at no location was any clear throughgoing fault found, and at three of the locations little or no morphological expression of the fault existed. Instead the active trace was identified by the presence of a series of en echelon fissures, sigmoidally or erratically shaped in map view, each 1–5 m long and with maximum opening of 1–5 mm. The separation of these fissures along the strike of the fault varied from closely spaced with their leading and trailing ends

Figure 4. (a) Triggered slip follows the arrival of surface waves (least-squares fit to onset of triggered slip 2.2 ± 0.1 km/s). (b) The time between the onset of triggered slip and (c) its completion (slip duration) increases with epicentral distance (0.6 s/km) as does, the delay to the time of maximum local aseismic slip velocity (1.6 km/s). (d) Log plot of the modulus of triggered slip amplitude versus log distance shows a general decay in maximum amplitude with distance, but with exceptions based on the history of slip in certain fault segments. The color version of this figure is available only in the electronic edition.

overlapping to a spacing between contiguous fissures of 2–4 m. At three locations (GB, GS, and GT), our chosen sites were on sequences of unmapped fissures interpolated between those on the preliminary map of surface fissuring (Kendrick et al., 2019) in which Coulomb failure stresses were anticipated to have brought the Garlock fault closer to failure (Barnhart et al., 2019). The extensometer GT installed near Trona Road was placed on the westernmost location where we encountered triggered fissuring. The tarmac of the nearby Trona Road was undisturbed by the earthquake, but a clear sequence of recent en echelon fractures was identified cutting the surface of a silt-rich soil and an off-road track to its west. The site GD was selected from its morphology, a hillside bench bordered by a modest shutter ridge ≈100 m west of a paleoseismic trench excavated by Dawson et al. (2003). We found no evidence for triggered surface fractures at this location.

TABLE 2 Epicentral Distance (km), Calculated Surface-Wave Arrival Time (s after Mainshock), Interpolated Onset of Slip (s), Time (T_{max}) of Maximum Velocity (mm/s) and Duration of Triggered Slip (s)

Location	Epicentral Distance (km)	<i>S</i> Wave	Onset ±30	Duration	Velocity (mm/s)	T _{max}
QW30	271.2	77.5	135	120	2.8	167
QE30	272.0	77.7	120	120	3.4	146
IR30	284.0	81.1	210	120	0.008	247
NS45	289.6	82.7	105	188	0.08	259
FE30	300.6	85.9	142	180	0.19	169
SC30	301.9	86.3	113	180	0.24	130
SC72	301.9	86.3	150	180	0.07	250
DU30	307.7	87.9	-	_	_	-
SH30	308.1	90.0	-	_	_	-
XMR1	332.1	94.9	120	150	0.03	160
SU30C	358.1	102.3	130	351	0.005	253
SU30I	358.1	102.3	-	300	0.006	-
RR45	383.9	109.7	136	300	0.057	196

The onset time listed is interpolated to 10 s between 1 min samples. Because of the uncertain slope of initial offset and the 1 min sampling interval we assign to this time pick an uncertainty of ± 30 s. The time of maximum slip velocity (T_{max}) is also indicated to the nearest half-minute corresponding to the time of the maximum velocity between two contiguous samples. Although absolute time is not known relative to UTC to better than 5 s, the relative timing during slip is precise to 1 s.

TABLE 3

Location of Extensometers in the Ridgecrest Epicentral Region

Site	Latitude	Longitude	Date	<i>L</i> (m)	Azimuth	Location
R7(35)	35.5960	117.4019	19 July	4	123	$M_{\rm w}$ 7.1, 20 m south of Pinnacle Road
RB(30)	35.6189	117.5722	9 July	14	62	$M_{\rm w}$ 6.4. 50 m north of Randsburg Wash road
RA(30)	35.6189	117.5722	22 July	≈2	62	M_{w} 6.4, 52 m north of Randsburg Wash road
GS(30)	35.5022	117.4678	20 July	10.5	100	Garlock, Searles Valley, 10 mm cracks
GT(30)	35.4695	117.5919	21 July	9.8	97	Garlock, near Trona Road, 5 mm cracks
GB(30)	35.5239	117.3731	22 July	4	130	Garlock, 8 mm cracks
GD(30)	35.4434	117.6832	29 July	8	103	Garlock, no surface cracks

The numbers in parenthesis in the first column indicate the local obliquity of the extensometer to the fault ± 5 °. The azimuth of the extensometer is indicated in degrees northeast ± 5 °.

The largest observed epicentral afterslip signal (1.1 mm in four months) occurred on the $M_{\rm w}$ 6.4 rupture (Fig. 5). Elsewhere, signals across faults were less than 0.1 mm. These small signals are not symptomatic of afterslip in the sense of localized, continued slip on surface faults. Two observations suggest that the extensometers provide a measure of epicentral surface strain relaxation (Fig. 6).

The first observation follows from data recorded by two extensometers (RA and RB) that were installed across the $M_{\rm w}$ 6.4 rupture to test whether the recently formed main fissure

represented a weak inclusion separating two elastic quarter spaces. The first (RB activated 9 September 2019 02:11) was 14 m long and crossed a branch of the main rupture, a spectacular pair of 20 cm wide open fissures, including five or more hairline fissures to their east, each with a few millimeters of displacement (Fig. 6a). Eleven days later we installed a 2 m long extensometer (RA activated 22 September 2019 13:47) in the same azimuth 2 m to the north of RB spanning just the open fissures. Anticipating

amplified displacements across the open fissure with this shorter instrument, we were surprised to measure displacements that were approximately consistent with uniform strain. During the following few months, the short instrument measured extension at 0.63 mm/yr and the longer instrument at 3.03 mm/yr. Thus, the 2 m wide region spanning the main fissure and the 14 m wide region spanning the hairline cracks behaved as though they were part of a uniform elastic material extending by $4-6~\mu strain/week$ at azimuth N62°W. If this is the case the offsets at the time of local aftershocks captured by extensometer

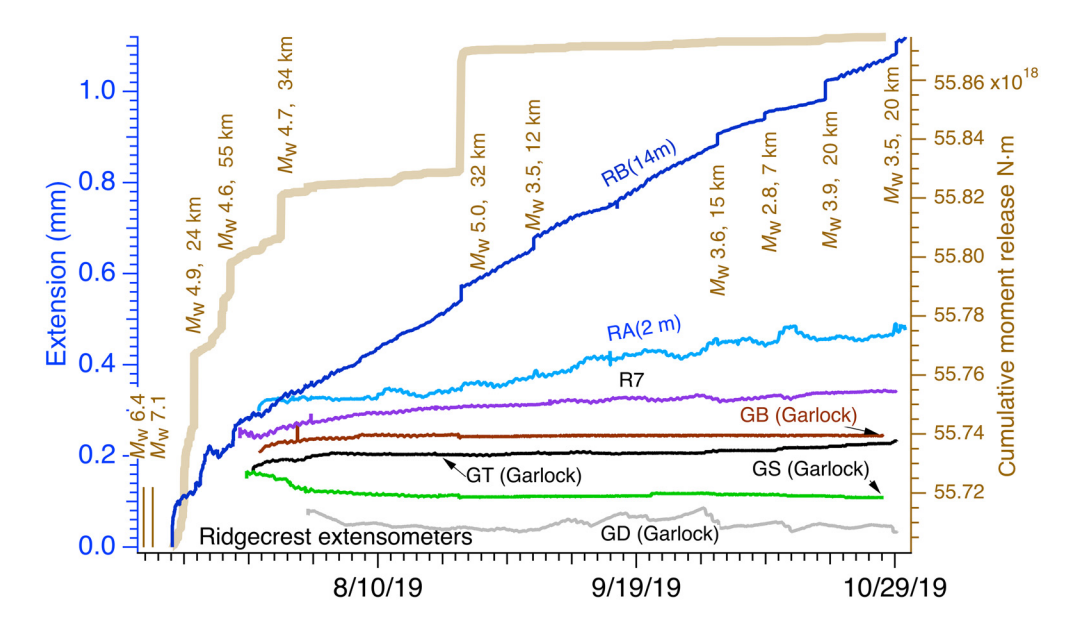


Figure 5. Sixteen weeks of extensometer data from the epicentral region, compared to cumulative seismic moment release (right axis). For locations, see Figure 1 and Table 3. Significant aftershocks and distances from the RB creepmeter are indicated at the time of offsets. Less than 1.1 mm of slip has occurred on the main ruptures and less than 0.1 mm on the Garlock fault. The ratio of the almost linear trends of RB (3.03 mm/yr) and RA (0.63 mm/yr) is 4.8:1, which approximates the ratio of their lengths (7:1) suggesting that they record uniform strain of $5 \pm 1~\mu strain/week$ in the vicinity of the M_w 6.4 rupture. The color version of this figure is available only in the electronic edition.

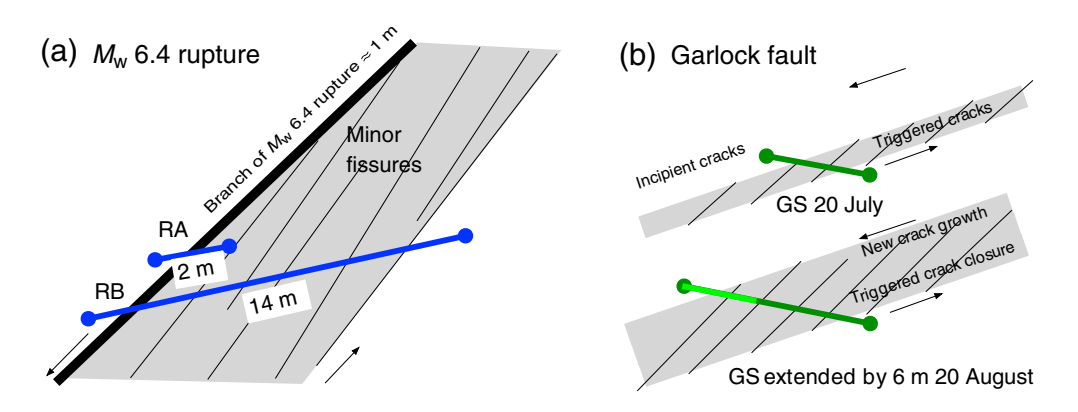


Figure 6. Schematic map views of three of the extensometers in the Ridgecrest region. (a) Displacements measured by RA and RB are roughly proportional to their lengths indicating that they measured approximately uniform strain in the two months following the earthquakes. (b) The GS extensometer on the Garlock fault initially measured a right-lateral signal that we diagnosed as en echelon crack closure due to the development of incipient cracking outside the aperture of the instrument. Minor sinistral opening was observed after we lengthened the sensor from 10.5 to 16.5 m. The color version of this figure is available only in the electronic edition.

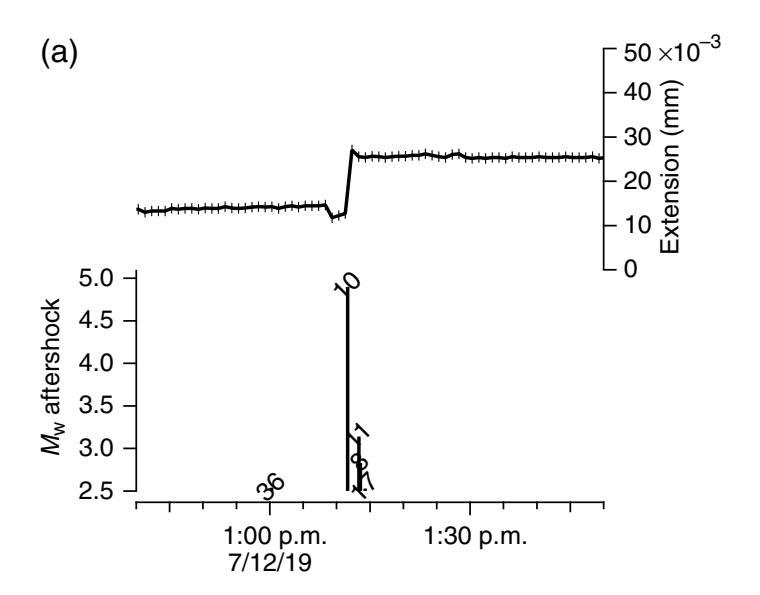
RB, if they are not artifacts in the extensometer, represent strain steps (amplitude $\leq 4~\mu strain$), rather than triggered slip on the $M_{\rm w}~6.4~surface~rupture$. Interferometric Synthetic Aperture Radar (InSAR) observations in the same period of time centered on the 500 m surrounding the RA and RB extensometers are

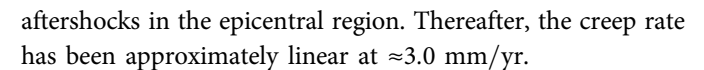
consistent with this strain rate (compared to K. Wang and R. Bürgmann, unpublished manuscript, 2019, see Data and Resources).

The second observation comes from extensometer GS that was located across a ≈3 m wide zone of left-lateral en echelon tension fissures on the Garlock fault (Fig. 6b), and in the following 10 days recorded a 50 μ m dextral creep signal (Fig. 5). A week after installation, we discovered that these initial en echelon cracks had doubled in length to the north, increasing the zone of faulting to a ≈6 m wide zone that now extended outside the aperture of the extensometer. On 20 August, suspecting that the dextral signal here might in part be due to the relaxation of the width of the original cracks as new cracks developed, we added an additional 6 m to the length of the original extensometer to embrace the newly extended cracks. No further dextral signals were observed, and the subsequent signal has been close to zero. These observations suggest that surface cracks were dynamically induced during strong shaking, but that subsequent displacements record the response of surface materials as they adiusted to local stresses shallower than tens of meters, with no continuing localized strain at depth. The absence of continued extension on any of the Garlock fault creepmeters or of afterslip in the InSAR imagery on the southern ends of the Ridgecrest ruptures indicates

that no deep-seated slip was induced on the Garlock fault by the Ridgecrest sequence.

We note that in the first few weeks, the observed RB signal initially decayed with an approximate 16-day time constant similar to the decay in cumulative moment release from





Triggered Slip on Ridgecrest Ruptures Caused by Aftershocks

A number of $\leq 30 \ \mu m$ displacement events on the $M_{\rm w}$ 6.4 rupture were triggered by large aftershocks (Fig. 7a). The Little Lake $M_{\rm w}$ 5.0 aftershock (22 August 2019 20:49:50, 35.907° N, 117.709° W) at a hypocentral distance of 32 km caused abrupt offsets on both RA and RB (9 and 34 μ m corresponding to strains of ≈ 4 and $\approx 2.4 \mu strain$). The strain derived by the shorter instrument is subject to large uncertainties because the footprint of the buried tripod anchor is large compared to the length of the instrument. A nearby $M_{\rm w}$ 4.9 aftershock on 12 July (13:11:37 UTC, 35.638° N, 117.585° W) caused extension of 11 μ m but was preceded by a 3 min contractive precursor of 3 μ m (Fig. 7b). This precursor is unique within the data, but because it is equivalent to the least count sensitivity of the 12-bit transducer, it is considered too small to be significant. The similar amplitude and polarity of the six triggered displacements identified in Figure 5, however, are difficult to distinguish from instrumental artifacts (stiction) and for this reason have not been analyzed in detail. Triggered offsets on other extensometers in the area were rare.

Afterslip and Creep Events in the Coachella Valley Following Triggered Slip

The Ridgecrest sequence resulted in triggered slip in the Mecca Hills, as detailed earlier, but slip continued for several weeks on two creepmeters located 870 m apart (QW and QE) after the earthquake at reducing rate (Figs. 8 and 9). In addition, accelerated slip on Durmid Hill persisted for two months. This form of afterslip following triggering was first reported after the 2017 $M_{\rm w}$ 8.2 Chiapas earthquake (Timoyeyeva *et al.*, 2019). In the first few days of this local (triggered) afterslip, creep events

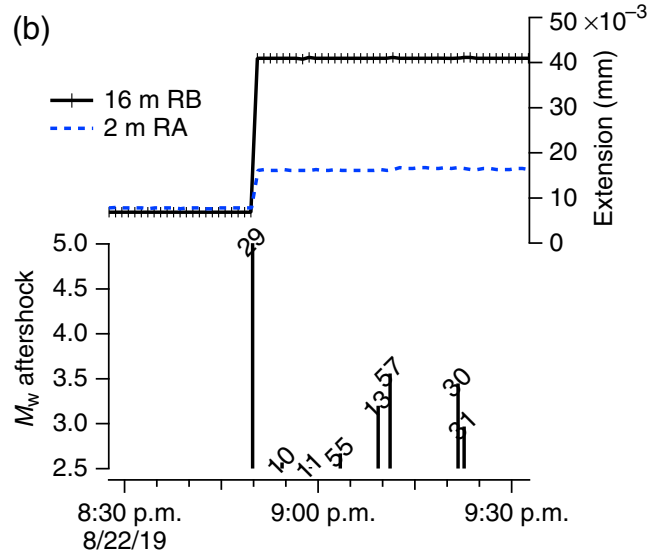
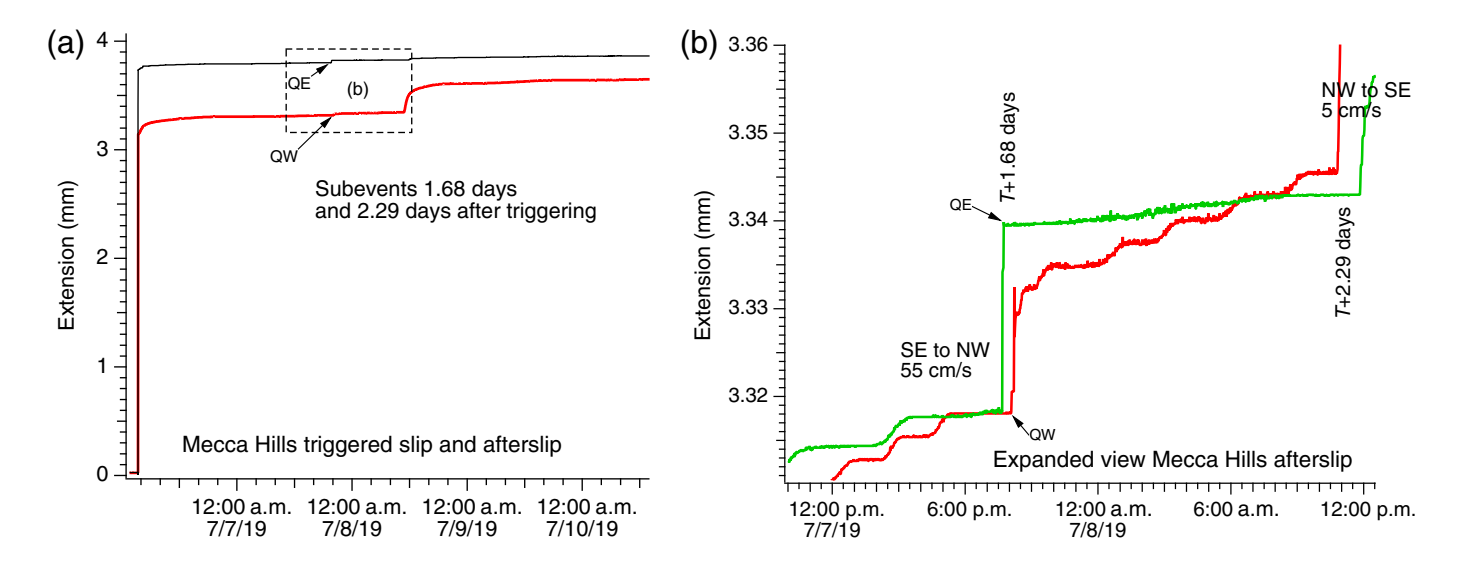


Figure 7. Sinistral offsets on the $M_{\rm w}$ 6.4 rupture caused by $M_{\rm w}$ 4.9 and 5 aftershocks. Oblique numbers indicate hypocentral distances (in kilometers) of aftershocks from the RA/RB extensometers. Tick marks correspond to sample times. (a) An intriguing dextral precursor precedes the $M_{\rm w}$ 4.9 aftershock on 12 July by >2 min (RA was installed 10 days later). (b) The extensional strain changes (but not the displacements) are recorded with similar amplitude on RA and RB at the time of the $5 < M_{\rm w} < 5.1$ Little Lake aftershock on 22 August. The color version of this figure is available only in the electronic edition.

propagated first to the northwest at 55 cm/s (47 km/day) and then to the southeast at 5 cm/s (4.32 km/day). These different velocities may represent the phase velocities of upward-propagating creep events from deeper levels on the southern San Andreas fault triggered by the Ridgecrest earthquakes.

Triggered slip at Salt Creek did not occur within minutes of the arrival of the surface waves from the $M_{\rm w}$ 6.4 earthquake, but 20 μ m of abrupt slip occurred after a 2.2 hr delay. We attribute this delay to triggered slip occurring nearby on the fault and propagating toward Salt Creek in the two hours following the event. Slip was incremented a further 0.6 mm within 5 min of the $M_{\rm w}$ 7.1 earthquake, but slip continued at a mean rate of 4.7 mm/yr for the succeeding two months, releasing a further 0.8 mm of slip on the fault (Fig. 9). The surface creep rate at FE30 also increased after the Ridgecrest triggering episode. Similar slip occurred at DU30; however, in this case, an increase in creep rate is apparent before the instrument malfunctioned in early June that renders a change of rate following triggered slip uncertain. Cumulative slip of 0.11 mm was triggered at DU30 by two small earthquakes near Bombay Beach (M_w 3.8 16 September 2019, 33.362° N, 115.789° W and $M_{\rm w}$ 3.6, 19 September) accompanied by a number of aftershocks of smaller magnitude, which subsequently led to the refurbishment of the moribund North Shoreline fault creepmeter (SH, Fig. 1). Although microearthquakes occur in this



region and on the Brawley seismic zone every few years, the association of this particular swarm with increased creep on the nearby southernmost San Andreas fault is considered significant.

Discussion

The Ridgecrest earthquakes were unusual for the extent of surface fissuring on unmapped faults in the epicentral area (Kendrick et al., 2019) and, documented here, as far south as the San Andreas fault in the Mecca Hills and Durmid Hill. The triggered slip we report is all aseismic in nature, the sole evidence for its occurrence being the observation of relative displacements along the surface of the disturbed fault. If we propose that slip less than the resolution of our sensors $(2 \mu m)$ as an indicator of an absence of triggering, five locations beyond 270 km did not respond to the $M_{\rm w}$ 6.4 earthquake, but all 11 teleseismic instruments out to 384 km responded to the $M_{\rm w}$ 7.1 earthquake, albeit with amplitudes smaller than those reported hitherto. Given this observation, it would appear reasonable to suppose that minor triggered slip may have occurred invisibly on many unmonitored faults in California and that similar remote triggering may be common elsewhere (see, for example, Victor et al., 2018).

One concern with this supposition is that the instruments themselves may be disturbed by teleseismic shaking. Stiction is indeed present in the tensioned rod and rotary sensor as mentioned in the Introduction, but this can readily be distinguished from slip in the fault zone by its transient (0.1-2 s) duration compared to the prolonged duration of induced fault creep, at some locations taking many days (Figs. 8 and 9). At just one location (IR30, Fig. 3c) was triggered slip complete in less than one minute, and even here it is apparent that slip may have commenced in the preceding minute. Moreover, of the seven new extensometers installed in the epicentral region that were exposed to hundreds of local $M_{\rm w} > 2.5$ aftershocks for two months, triggered slip was rare. Examples are shown in Figure 7. Triggered slip on the Superstition Hills fault recorded

Figure 8. (a) Four days of afterslip recorded by the Mecca Hills creepmeters QE and QW. (b) An expanded view of two propagating creep events that start 1.68 days and 2.29 days after initial triggered slip (Fig. 3a,b), the first propagating northwest at 55 cm/s and the second propagating southeast at 5 cm/s. The step-like nature of the plot is caused by the 16-bit digitization of 12-bit increments ($\approx 2 \mu m$) from the outputs of the Hall sensors. The color version of this figure is available only in the electronic edition.

by independent systems of different design was similar in amplitude and sign (Fig. 3k). Finally, at most locations (15 of the 18 sensors), triggered slip occurred with the same polarity as secular slip on the local fault.

At three locations, however, we recorded retrograde slip in the form of sinistral slip on dextral faults and dextral slip on sinistral faults. We account for this at two of the locations (NS and RR) where the sense of motion is similar to a seasonal reversal in direction that is seen occasionally at these sites and is usually associated with hydrologic or seasonal thermal changes. This was not the case at the site IR where the retrograde slip direction is small (-8 μ m) and recovers to a dextral offset of $+3 \mu m$ after 1 day. This particular sensor being located near a seasonal stream was designed to function when submersed and is unique among the 18 extensometers in that it includes an idler pulley arranged to change the tension direction between horizontal rod and vertical sensor by 90°. We attribute the measured sense of motion and its recovery to an artifact in the bearings of this idler pulley. At the Garlock site GS in the epicentral region, we attribute apparent retrograde slip to the growth of fissures responding to triggered slip at depth (Fig. 6b).

Triggered slip is generally considered a surface process because it is measured by surface extensometers. From the Mecca Hills and Durmid Hill data recorded here, however, it would appear that it must also occur in the subsurface, with some aseismic fault offsets propagating to the surface as discrete

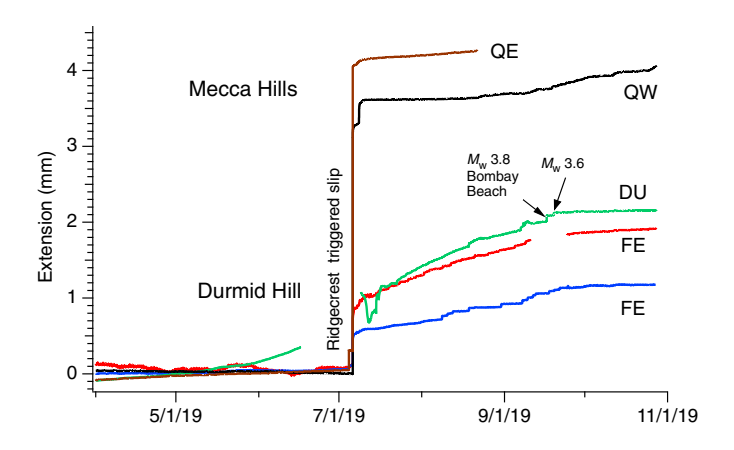


Figure 9. Rate changes on Durmid Hill following the Ridgecrest earthquakes. For two months prior to the earthquakes creepmeters, FE30 and SC30 recorded essentially zero slip (a malfunction in DU30 occurs a few weeks before the earthquakes). For more than two months following the earthquakes their rates increased to \approx 4 mm/yr, a rate that is more than double the mean creep rate of previous years. On 16 and 19 September, the DU30 creepmeter (noisy immediately following repairs on 7 July) recorded 0.11 mm of cumulative triggered slip at the time of $M_{\rm w}$ 3.8 and 3.6 earthquakes near Bombay Beach. The color version of this figure is available only in the electronic edition.

creep events over days (Fig. 8) or slowly at decreasing creep rates over weeks (Fig. 9). The southernmost San Andreas fault responded similarly following the $M_{\rm w}$ 8.2 Chiapas earthquake in 2017 (Tymofyeyeva *et al.*, 2019) when triggered slip doubled in amplitude in the following month by a process of decaying afterslip and was followed after three months by a southward propagating creep event with 0.5 mm amplitude.

Surface creep on the southern San Andreas fault accompanying surface waves from the Chiapas earthquake is calculated from surface deformation fields in Tymofyeyeva et al. (2019) to have occurred at depths shallower than 2.5 km on Durmid Hill and shallower than 0.5 km in the Mecca Hills. Slip was triggered slip by both the Ridgecrest $M_{\rm w}$ 6.4 and by the $M_{\rm w}$ 7.1 earthquakes, and the first earthquake incompletely released shear strain locally accumulated near the fault since the Chiapas earthquake or earlier. The larger amplitude surface waves of the $M_{\rm w}$ 7.1 event at each location released more slip than the $M_{\rm w}$ 6.4 event. This additional slip is consistent with the calculations of Tymofyeyeva et al. (2019). However, because surface slip is almost linearly proportional to the depth of a freely slipping dislocation on a fault subject to uniform shear strain in a uniform half-space, the ratio of slip amplitudes released in the two triggered events can be considered to represent slip to different depths given by the ratio of observed slip amplitudes. The observed ratios of slip at each creepmeter location appear to be site specific on the southern San Andreas fault (Table 1). If we assume that the maximum depth of triggered creep in the Chiapas $M_{\rm w}$ 8.2 and Ridgecrest $M_{\rm w}$ 7.1 earthquakes was similar, we can estimate the approximate depths of triggered creep in the $M_{\rm w}$ 6.4 earthquake. At QU30 where the depth of slip in the Chiapas event was calculated to be 0.5 km, a ratio of 12.5 is obtained, implying that slip in the $M_{\rm w}$ 6.4 event was confined to the uppermost 40 m of the fault. At FE30, where the slip depth was inferred to be 2.5 km in the Chiapas triggering episode, the ratio is 7.3, implying that slip shallower than 340 m was triggered by the $M_{\rm w}$ 6.4 event. At SC30 just 400 m to the southeast of FE30 the observed ratio is 2.2 implying slip to 1.1 km depth in the first event. These calculations apply only to the instantaneous triggered slip within a day of each event. Subsequent slip (Fig. 9) presumably occurs throughout the shallow fault, either in the form of discrete propagating dislocations (Fig. 8) or as slow uneventful creep.

Within a time span of less than 2 hr in August 2012, two $M_{\rm w} > 5$ earthquakes on the Brawley fault triggered 0.15 mm of cumulative slip on the Superstition Hills fault 15-20 km to their west that would appear to be inconsistent with the above interpretation (Hauksson et al., 2013). In this swarm 0.1 mm of slip accompanied an $M_{\rm w}$ 5.3 earthquake, but only 0.05 mm of additional slip accompanied the larger succeeding $M_{\rm w}$ 5.4 mainshock. The mainshock was ≈3 km further from the Superstition Hills fault, but both mainshock and foreshock were interpreted to lie on the same fault, placing the creepmeter (SU30) almost precisely on a nodal plane. Unlike the teleseismic surface-wave triggering we discuss in the Ridgecrest and Chiapas earthquakes, triggered slip on the Supersitition Hills fault by earthquakes on the Brawley fault occurs essentially in the near field and presumably is induced by *P* and/or *S* waves. The authors assumed that in this case slip triggered by the foreshock had already partly released shear strains local to the Superstition Hills fault, leaving little to be released in the mainshock.

Teleseismic triggering is clearly a dynamic process because the static strains at >270 km distances are small (Wei et al., 2015). That maximum triggered slip has again occurred on transpressive segments of the San Andreas fault adjoining the Salton Sea, with negligible slip in the intervening North Shore segment (Bilham and Williams, 1985), indicates that some fault segments are particularly sensitive to triggering. Increased pore pressures were identified as possibly important by Sieh and Williams (1990), and it is possible that pore pressures near the fault are selectively increased during the passage of surface waves, by processes similar to those induced by liquefaction. The prolonged duration of slip at distant sites may be related to the longer duration and longer wavelengths of dispersed surface waves at these distances. That surface afterslip following triggered slip has not been noted until recently on the southern San Andreas fault may be related to the longer wavelengths of surface waves responsible for teleseismic triggering slip in the 2017 Chiapas and 2019 Ridgecrest earthquakes (3000 and 270-380 km distances) compared to previous triggered slip here from earthquakes that have occurred at

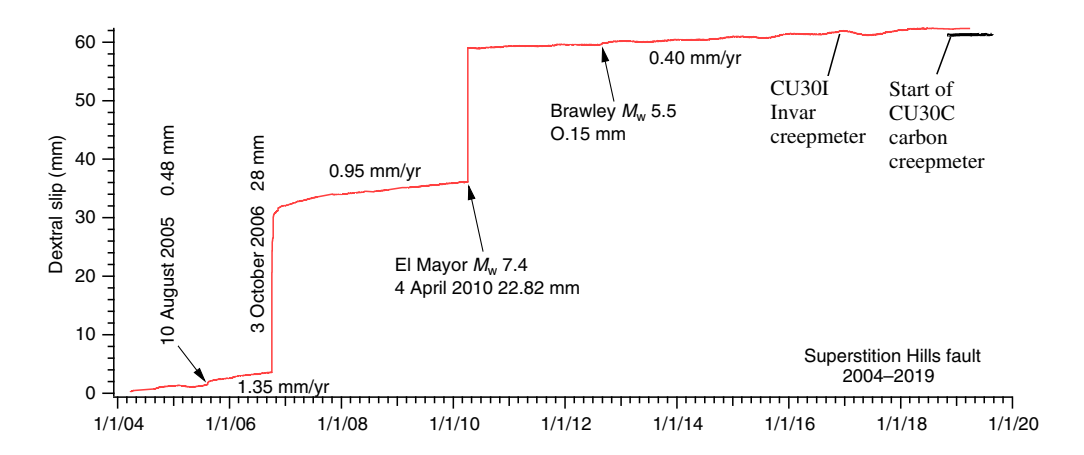


Figure 10. Fifteen years of creep data from the Invar creepmeter SU30I on the Superstition Hills fault showing a slowing of background rate and the absence of significant triggered slip since the 2010 El Mayor–Cucapah earthquake. Creep events 2004–2008 occurred spontaneously. The Invar creepmeter was terminated a few weeks after the Ridgecrest earthquakes following a period of overlap with a new carbon rod creepmeter (SU30C) at the same location. The color version of this figure is available only in the electronic edition.

distances closer than 200 km (Cohn et al., 1982; Bodin et al., 1994; Rymer et al., 2011; Wei et al., 2011, 2015).

Triggered seismicity not associated with surface fault slip in the Salton Sea area has been reported from major earthquakes at considerably greater distances than discussed here (Castro *et al.*, 2017). The delayed afterslip observed on the southern San Andreas fault following the Ridgecrest and Chiapas earthquakes provide additional support for the mechanisms of delayed triggering of earthquakes proposed by Shelly *et al.* (2011).

The absence of significant triggered slip on the Superstition Hills fault, and its absence also in the Chiapas earthquake (Tymofyeyeva et al., 2019) is perhaps surprising because this fault has in the past also proven to be sensitive to triggering (Wei et al., 2015). It slipped spontaneously 28 mm on 3 October 2006, and 22.82 mm in the 4 April 2010 $M_{\rm w}$ 7.4 El Mayor-Cucapah earthquake (Rymer et al., 2011), and a mere 0.15 mm in the nearby Brawley earthquake of 2012 (Hauksson et al., 2013). The 2010 El Mayor triggered slip was remarkable (Fig. 10) in that all the slip occurred between two 15 min samples with no afterslip on the fault in the following days or weeks, unlike the persistent decaying slip that has followed previous Superstition Hills triggered events. Prior to the El Mayor-Cucapah earthquake, the creep rate was 0.95 mm/yr, and, in the following nine years, its rate has reduced to 0.4 mm/yr. It is possible that in 2010 the Superstition Hills fault was induced to overshoot its local stressing rate by the application of a combination of static and transient dynamic stresses. If this is the case, it may be many years before significant triggered slip on the Superstition Hills fault will accompany a future strong nearby earthquake.

No significant slip occurred on any of the six fault segments that we instrumented in the Ridgecrest epicentral region. Circumstantial evidence suggests that these time series (Fig. 5) record strain rather than discrete slip on faults. For example, the pair of instruments RA and RB installed across the $M_{\rm w}$ 6.4 rupture (Fig. 6a) recorded different displacements, but when normalized by their lengths, the signals correspond approximately to a strain rate of $\approx 1 \, \mu strain/day$, similar strains measured by InSAR in the postseismic period (K. Wang and R. Bürgmann, unpublished manuscript, 2019, see Data and Resources).

Localized surface offsets along the Garlock fault visible on the ground and in InSAR

scenes plus the inferred enhanced Coulomb failure along that part of the Garlock fault in the southwest quadrant between the $M_{\rm w}$ 6.4 and 7.1 Ridgecrest ruptures led us to install four extensometers along its surface trace in anticipation of continued slip. Following an initial settling period, these extensometers have measured less than 0.1 mm of cumulative displacement. A transient retrograde slip detected at one of these sites (GS) was interpreted to have been caused by the growth of fissures associated with the relaxation of local strain (Fig. 6b).

Conclusions

We report data acquired from 19 fault-zone extensometers recording at one sample per minute. Eleven in southern California and one near Hollister were operating during the Ridgecrest sequence, and seven were installed subsequently in the meizoseismal region. The southern California network confirms that triggered slip follows the arrival of surface waves. We identify maximum slip rates of 3.4 mm/ min that occur within one or two minutes of the arrival of surface waves with triggered slip continuing for up to 6 min at 380 km distances. Least-squares fit to the time of occurrence of the onset of triggered slip and maximum triggered slip velocity yielded propagation rates of $2.2\pm0.1~\rm km/s$ and $1.6\pm0.2~\rm km/s$, respectively, but the sparse 1 min sample rate adds additional uncertainties.

Afterslip on discrete faults appears to be absent in the southern part of the Ridgecrest epicentral region. We interpret the small observed signals observed here as microstrain surface relaxation, rather than as slip on discrete surface ruptures. Specifically, the Garlock fault appears locked for the 40 km region we have instrumented.

An unexpected aspect of triggered slip on the southern San Andreas fault is that for several months following teleseismic

shaking the fault exhibited an increase in surface slip rate that continued with slowly decaying rate. Prolonged afterslip also followed slip triggered by the Chiapas earthquake in 2017. This behavior appears to be a style of response to dynamic triggering that has not been observed previously on surface faults, but which we attribute to the propagation of subsurface triggered slip to the surface and along the fault. Delays in triggered seismicity have been ascribed to creep processes here and elsewhere (Shelly et al., 2011; Castro et al., 2017), but to our knowledge our creep observations in 2017 and 2019 constitute the first direct observations of this process. A shallow swarm of earthquakes, the largest of which was M_w 3.8 (33.362° N, 115.789° W), occurred near Bombay Beach at the southernmost end of the southern San Andreas fault on 16 September 2019, subsequent to 2 mm of aseismic slip developing on the San Andreas fault through Durmid Hill.

Considerable insight into fault behavior was obtained from instruments poised to capture the slip process operating prior to and during the Ridgecrest sequence, compared to information on fault processes from those installed after the earthquakes. This conclusion underlines an opinion recently voiced by Ben-Zion (2019) that earthquake studies would benefit considerably from anticipatory *in situ* fault instrumentation to capture future slip. In the Discussion section, we quantify the unexpected temporal evolution of triggered slip that would have been much improved with faster sampling rates and higher resolution data. The technology for such measurements is readily available.

Data and Resources

The creep data described in this article are available from the UNAVCO archive at the following website https://www.unavco.org/data/strain-seismic/creep/ (last accessed November 2019). The unpublished manuscript by K. Wang and R. Bürgmann (2019), "Co- and early postseismic deformation due to the 2019 Ridgecrest earthquake sequence constrained by Sentinel-1 and COSMO-SkyMed SAR data," submitted to Seismol. Res. Lett.

Acknowledgments

The U.S. Geological Survey (USGS) 04HQAG0008 funded the creepmeters in the Coachella Valley for the period 2004–2012 (Fig. 10). The 2019 study was funded by the National Science Foundation (NSF) RAPID-EAR1941558, by the USGS Earthquake Science Center Deformation Project, and with support from NSF EAR 1650364. The authors thank Dave Mencin for assistance in assembling the Ridgecrest creepmeters, Roland Bürgmann for critically reviewing the text; Sally McGill, Ben Brooks, and Jose Mora for enthusiastic field support; and Kate Scharer and Sue Hough for coordinating Ridgecrest field work. Sites for epicentral creepmeters were selected following discussions with Ben Brooks, Tom Dawson, James Dolan, Ken Hudnut, Craig Jones, Mark Murray, Maxime Mareschal, Tom Rockwell, Gordon Seitz, Jerry Treiman, and Ryan Turner, some of whom helped with the digging.

References

- Barnhart, W. D., G. P. Hayes, and R. D. Gold (2019). The July 2019 Ridgecrest, California earthquake sequence: Kinematics of slip and stressing in cross-fault ruptures, *Geophys. Res. Lett.* doi: 10.1029/2019GL084741.
- Ben-Zion, Y. (2019). A critical data gap in earthquake physics, Seismol. Res. Lett. **90**, no. 5, 1721–1722, doi: 10.1785/0220190167.
- Bilham, R. (1989). Surface slip subsequent to the 24 November 1987 Superstition Hills, earthquake, California, monitored by digital creepmeters, *Bull. Seismol. Soc. Am.* **79**, no. 2, 425–450.
- Bilham, R. (2005). Co-seismic strain and the transition to surface afterslip recorded by creepmeters near the 2004 Parkfield epicenter, *Seismol. Res. Lett.* **76**, no. 1, 49–57.
- Bilham, R., and P. Williams (1985). Sawtooth segmentation and deformation processes on the San Andreas Fault, California, *Geophys. Res. Lett.* **12**, 557–560.
- Bodin, P., R. Bilham, J. Behr, J. Gomberg, and K Hudnut (1994). Slip triggered on southern California faults by the Landers, earthquake sequence, *Bull. Seismol. Soc. Am.* **84**, no. 3, 806–816.
- Castro, R. R., R. Clayton, E. Hauksson, and J. Stock (2017). Observations of remotely triggered seismicity in Salton Sea and Coso geothermal regions, Southern California, USA, after big (Mw > 7.8) teleseismic earthquakes, *Geofis. Int.* 56, no. 3, 269–286.
- Cohn, S. N., C. R. Allen, R. Gilman, and N. R. Goulty (1982). Preearthquake and postearthquake creep on the Imperial fault and the Brawley fault zone, in *The Imperial Valley, California*, *Earthquake of October 15*, 1979, C. E. Johnson, C. Rojahn, and R. V. Sharp (Editors), Geological Survey Professional Paper 1254, U.S. Government Printing Office, Washington, D.C., 161– 167.
- Dawson, T. E., S. F. McGill, and T. K. Rockwell (2003). Irregular recurrence of paleoearthquakes along the central Garlock fault near El Paso Peaks, California, *J. Geophys. Res.* 108, no. B7, 2356, doi: 10.1029/2001JB001744.
- Hauksson, E., J. Stock, R. Bilham, M. Boese, X. Chen, E. J. Fielding, J.
 Hutton, L. M. Jones, H. Kanamori, P. M. Shearer, et al. (2013).
 Report on the August 2012 Brawley earthquake swarm in Imperial Valley, Southern, California, Seismol. Res. Lett. 84, no. 2, 177–189.
- Jänecke, S. U., D. K. Markowski, J. P. Evans, P. Persaud, and M Kenney (2018). Durmid ladder structure and its implications for the nucleation sites of the next M > 7.5 earthquake on the San Andreas fault or Brawley seismic zone in southern California, *Lithosphere* doi: 10.1130/L629.1.
- Kendrick, K. J., S. O. Akciz, S. J. Angster, J. Avouac, J. L. Bachhuber, S.
 E. Bennett, K. Blake, S. Bork, B. A. Brooks, P. Burgess, et al. (2019).
 Geologic observations of surface fault rupture associated with the Ridgecrest M6.4 and M7.1 earthquake sequence by the ridgecrest rupture mapping group, Poster Presentation 217 at 2019 SCEC Annual Meeting, Palm Springs, California, 8–11 September 2019.
- Louie, J. N., C. R. Allen, D. C. Johnson, P. C. Haase, and S. N. Cohn (1985). Fault slip in southern California, *Bull. Seismol. Soc. Am.* **75**, 811–833.
- McGill, S., C. Allen, K. Hudnut, D. Johnson, W. Miller, and K. Sieh (1989). Slip on the Superstition Hills fault and on nearby faults associated with the 24 November 1987 Elmore Desert Ranch

- and Superstition Hills earthquakes, southern California, *Bull. Seismol. Soc. Am.* **79**, 362–375.
- Rymer, M. J., J. A. Treiman, K. J. Kendrick, J. J. Lienkaemper, R. J. Weldon, R. Bilham, M. Wei, E. J. Fielding, J. L. Hernandez, B. P. E. Olson, et al. (2011). Triggered surface slips in southern California associated with the 2010 El Mayor-Cucapah, Baja California, Mexico, earthquake, U.S. Geol. Surv. Open-File Rept. 2010-1333 and California Geol. Surv. Spec. Rept. 221, 62 pp., available at http://pubs.usgs.gov/of/2010/1333/ (last accessed November 2019).
- Schulz, S. S. (1989). Catalog of creepmeter measurements in California from 1966 through 1988, U.S. Geol. Surv. Open-File Rept. 89-650.
- Shelly, D. R., Z. Peng, D. Hill, and C. Aiken (2011). Triggered creep as a possible mechanism for delayed dynamic triggering of tremor and earthquakes, *Nature Geosci.* **4**, 384–388.
- Shifflett, H., M. G. Gray, R. Grannell, and B. L. Ingram, (2002). New evidence of the slip rate, renewal time, and late Holocene surface displacement, southernmost San Andreas Fault, Mecca Hills, California, *Bull. Seismol. Soc. Am.* 92, no. 7, 2861–2877.
- Sieh, K. E., and P. L. Williams (1990). Behavior of the southernmost San Andreas Fault during the past 300 years, *J. Geophys. Res.* **95**, 6629–6645.
- Tymofyeyeva, E., Y. Fialko, J. Jiang, X. Xu, D. Sandwell, R. Bilham, T. K. Rockwell, C. Blanton, F. Burkett, A. Gontz, and S. Moapoor (2019). Slow slip event on the southern San Andreas fault triggered

- by the 2017 Mw8.2 Chiapas (Mexico) earthquake, *J. Geophys. Res.* **124**, 9956–9975, doi: 10.1029/2018JB016765.
- U.S. Geological Survey and California Geological Survey (2006).
 Quaternary fault and fold database for the United States, available at http://earthquake.usgs.gov/hazards/qfaults/ (last accessed October 2019).
- Victor, P., O. Oncken, M. Sobiesiak, M. Kemter, G. Gonzalez, and T. Ziegenhagen (2018). Dynamic triggering of shallow slip on forearc faults constrained by monitoring surface displacement with the IPOC Creepmeter Array, *Earth Planet. Sci. Lett.* **502**, 57–73, doi: 10.1016/J.EPSL.2018.08.046.
- Wei, M., Y. Liu, Y. Kaneko, J. McGuire, and R. Bilham (2015). Dynamic triggering of creep events in the Salton Trough, Southern California by regional M ≥ 5.4 earthquakes constrained by geodetic observations and numerical simulations, *Earth Planet. Sci. Lett.* **427**, 1–10, doi: 10.1016/j.epsl.2015.06.044.
- Wei, M., D. Sandwell, Y. Fialko, and R. Bilham (2011). Slip on faults in the Imperial Valley triggered by the 4 April 2010 Mw 7.2 El Mayor-Cucapah earthquake revealed by InSAR, *Geophys. Res. Lett.* 38, no. 1, LXXXXX, doi: 10.1029/2010GL045235.

Manuscript received 1 October 2019
Published online 15 January 2020